Two-dimensional square buckled Rashba lead chalcogenides

Paul Z. Hanakata,[1,*] A. S. Rodin,[2] Alexandra Carvalho,[2] Harold S. Park,[3] David K. Campbell,[1,†] and A. H. Castro Neto[2]

[1]*Department of Physics, Boston University, Boston, Massachusetts 02215, USA*
[2]*Centre for Advanced 2D Materials and Graphene Research Centre, National University of Singapore, 6 Science Drive 2, 117546, Singapore*
[3]*Department of Mechanical Engineering, Boston University, Boston, Massachusetts 02215, USA*

We propose the lead sulphide (PbS) monolayer as a two-dimensional semiconductor with a large Rashba-like spin-orbit effect controlled by the out-of-plane buckling. The buckled PbS conduction band is found to possess Rashba-like dispersion and spin texture at the M and Γ points, with large effective Rashba parameters of $\lambda \sim 5$ eV Å and $\lambda \sim 1$ eV Å, respectively. Using a tight-binding formalism, we show that the Rashba effect originates from the very large spin-orbit interaction and the hopping term that mixes the in-plane and out-of-plane p orbitals of Pb and S atoms. The latter, which depends on the buckling angle, can be controlled by applying strain to vary the spin texture as well as the Rashba parameter at Γ and M. Our density functional theory results together with tight-binding formalism provide a unifying framework for designing Rashba monolayers and for manipulating their spin properties.

Introduction. Over the past two decades there has been a growing interest in materials with strong spin-orbit interaction (SOI), as they are of profound importance for a fundamental understanding of quantum phenomena at the atomic level and applications to spintronics. This relativistic interaction is linked to important effects such as Rashba, Zeeman, spin-Hall effect, and topological insulator (TI) states [1–4].

The spin-orbit splitting of the bands occurs in crystals without inversion symmetry, where it is known as the Dresselhaus effect and in two-dimensional (2D) structures or surfaces, where it is known as the Rashba effect, even though these can be seen as different manifestations of the same phenomenon [5]. However, suitable atomically thin 2D materials with a large Rashba coefficient are hard to find. To have Rashba-type spin splitting there are two key properties that should be present: strong SOI and broken inversion symmetry. In graphene and nonpolar two-dimensional materials, such as transition-metal dichalcogenides, breaking inversion symmetry is often achieved by application of out-of-plane electric fields or through interfacial effects [6–8]. Unfortunately, the respective spin splitting in graphene is rather small, rendering the spin polarization unusable at room temperature. Group IV and III-V binary monolayers (e.g., SiGe and GaAs) with buckled hexagonal geometry were found to have a Rashba-like spin texture; the band splitting, however, has a Zeeman-like splitting [9]. Spin splitting in WSe$_2$ monolayer is also of Zeeman type due to the out-of plane mirror symmetry (M_z: $z \rightarrow -z$) suppressing the Rashba term [7]. Transition-metal dichalcogenides with asymmetric surfaces, e.g., WSeTe, have a sizable Rashba splitting, but this does not coincide with the direct band gap [10]. A Rashba-type effect has been measured in few-layer samples of the topological insulator Bi$_2$Se$_3$, but this is attributed to the interactions with the substrate [11].

Recently, we proposed that a Rashba-like splitting can also be obtained in buckled heavy metal square lattices, where it is controlled by out-of-plane buckling and/or electric dipole [12]. However, materials in this class are almost always metals, which reduces the ways in which spins can be manipulated.

In addition to the study of spin splitting and texture in materials with strong SOI, several works have also investigated the orbital switching in topological insulators [13,14] and in *hexagonal* three-dimensional (3D) Rashba semiconductors [15,16]. Specifically, Cao *et al.* found that below the Dirac point the wave functions are more radial while above the Dirac point the wave functions are more tangential [13]. However, further studies for materials with different geometry (e.g., square) are still lacking.

Very recently, several studies have investigated the topological properties of the rocksalt structure materials, such as PbX ($X =$ Se, S, Te), in both monolayer and bilayer forms with no buckling [3,4,17]. In particular, Chang *et al.* have successfully grown few-layer SnTe and PbTe [18,19]. In this Rapid Communication, we study 2D lead chalcogenide PbX ($X =$ S, Se, Te) monolayers in square geometry with two atoms per primitive cell. For definiteness, we focus on lead sulfide PbS, but similar effects can be found for other lead chalcogenides and even heavy metals [12].

Using density functional theory (DFT), we find that buckled PbS monolayer possesses a strong Rashba splitting. In this polar material, the buckling direction can be reversed, leading to the reversal of the spin texture. Based on our DFT results we develop a tight-binding formulation of the buckled and planar 2D square lattice for PbS which is generally applicable for other similar materials (e.g., PbSe and PbTe). With this formalism, we are able to understand how the Rashba spitting depends on SOI strength, which in turn depends on the atomic species and the buckling angle, similar to the case of heavy metal square lattices [12]. Moreover, our theory provides an understanding of how spins and orbitals are coupled and how they can be controlled. These all together provide guidelines for designing and manipulating orbital-spin effects in Rashba monolayers.

Methods. Our findings are based on DFT calculations implemented in the QUANTUM ESPRESSO package [20]. We employed projector augmented-wave type pseudopotentials with Perdew-Burke-Ernzerhof within the generalized gradient

———————
*hanakata@bu.edu
†dkcampbe@bu.edu

approximation for the exchange and correlation functional [21]. The Kohn-Sham orbitals were expanded in a plane-wave basis with a cutoff energy of 100 Ry, and for the charge density a cutoff of 200 Ry was used. A k-point grid sampling grid was generated using the Monkhorst-Pack scheme with $16 \times 16 \times 1$ points [22], and a finer regular grid of $40 \times 40 \times 1$ was used for spin texture calculations. We used the modern theory of polarization [23] to calculate the spontaneous polarization implemented in the QUANTUM ESPRESSO package [20]. To compare the electric polarization of monolayer PbS to the typical bulk ferroelectrics, we approximate the thickness as twice the distance between the S and Pb atom which is roughly half of the lattice constant of bulk PbS. Similar approximations have also been used in several other works [24–26].

For electronic band structure calculations, the spin-orbit interaction was included using noncollinear calculations with fully relativistic pseudopotentials. To apply biaxial strains, we varied the in-plane lattice constants and let the system relax until the stress perpendicular to the plane is less than 0.01 GPa.

Structure, bistability, and ferroelectricity. Our first-principles calculations show that PbX monolayer has a buckled structure, which is a minimum of the energy surface, whereas the planar structure is a saddle point of the energy surface [27]. We found that the optimized buckled structure has a lower enthalpy of 120 meV compared to that of the optimized planar structure. The lattice constant a and buckling angle θ for the buckled (planar) structure are 3.74 Å (4.01 Å) and 21.6° (0°), respectively. The optimized planar lattice constant is close to the value reported in the study of planar PbS [17].

The energy barrier between the planar (paraelectric) and buckled (ferroelectric) is obtained by displacing the Pb and S atoms in the z direction while keeping the lattice parameters fixed at the values optimized for the the buckled (ferroelectric) phase. Using the fixed ferroelectric (buckled) lattice parameters, the energy barrier is 764 meV and the spontaneous polarization is Pol = 0.2 C/m^2. Since the calculation is carried out keeping the lattice parameters fixed at the values optimized for the buckled phase, the relative

energy of the paraelectric phase is overestimated. In fact, potential energy barriers in ferroelectric materials are usually strain dependent. For instance, Wang and Qian have shown that energy barriers in ferroelectric SnS, SnSe, GeS, and GeSe monolayers may increase or decrease depending on the strains [26]. To support our argument, we also calculated the path where the optimized paraelectric (planar) phase is used as the initial configuration. When the lattice parameters are fixed at the optimized paraelectric phase, the energy barrier is 51 meV and the spontaneous polarization is Pol = 0.1 C/m^2, as shown in the Supplemental Material. By fitting the energy surface to the fourth-order polynomial [28], we can calculate the coercive field given by $E_c = (4/3)^{(3/2)} E_{\text{barrier}}/\text{Pol}$. The calculated coercive field with the starting configuration from paraelectric (planar) and ferroelectric (buckled) are ~ 1 and ~ 10 V/nm, respectively. Applied electric fields of ~ 1 V/nm are achievable in current 2D experiments [29]. This suggests that PbS is suitable for a ferroelectric device as long as it is grown on its planar phase.

Band structure. Next we compare the band structure of planar PbS (PbS-p) and buckled PbS (PbS-b). PbS-p is a direct gap semiconductor with a small band gap of 0.2 eV. Because of the inversion symmetry, no spin splitting is observed. PbS-b is an indirect-gap semiconductor in which the minimum energy of the lowest conduction band is located near the M point and the maximum energy of the highest valence band is located near the Γ point. At both the M and Γ points, the conduction band shows a sizable Rashba splitting. The effective Rashba parameters, given by $\lambda = 2E_R/k_R$, where E_R is the difference between the lowest energy of the upper band and lower band and k_R is the shift in momentum space relative to the cone axis, are $\lambda = 1.03$ eV Å at Γ [Fig. 1(d)] and $\lambda = 5.10$ eVÅ at [Fig. 1(e)]. These values are comparable to those of 3D giant Rashba materials [1,2,30].

Origin of the spin splitting. A tight-binding formulation. Next, we use tight-binding formalism as a framework to understand the Rashba effects in lead chalcogenide monolayers. Numerical calculations show that the relevant bands
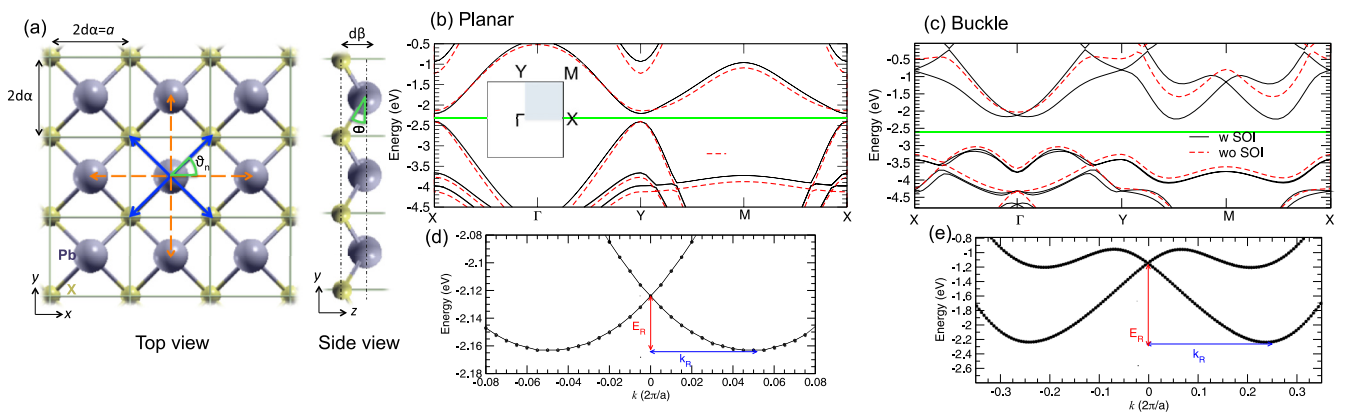

FIG. 1. (a) Structural visualizations of buckled PbS monolayer. Buckling angle $\theta = 0$ ($\beta = 0$) for planar structure. Blue and orange arrows indicate vectors connecting Pb and its first and second nearest neighbors, respectively. Band structure of monolayer PbS in planar (b) and buckled structure (c) along the high-symmetry lines of the Brillouin zone. Green lines indicate Fermi energy. There is no splitting in the planar structure because of inversion symmetry. In contrast, there is no mirror plane in z for the buckled structure resulting broken inversion symmetry, and this leads to band splitting. The calculated Rashba parameter at Γ (M) gives rise to a larger energy splitting between bands than other giant Rashba materials. Rashba-like dispersion at the Γ (d) and M points (e).

are composed almost exclusively of s and p orbitals of the constituent atoms, with d orbitals appearing in lower-energy valence bands, allowing us to neglect them [31]. This means that each atom introduces four (one s and three p) orbitals. While it is convenient to use p_x and p_y orbitals to write down the hopping elements, since we are including SOI in our model, it is helpful to go to a basis which is more natural for the angular momentum operators. We transform the basis as follows: $|1,1\rangle = (-|p_x\rangle + i|p_y\rangle)/\sqrt{2}$ and $|1,-1\rangle = (|p_x\rangle + i|p_y\rangle)/\sqrt{2}$. The new basis then for each 4×4 block is $|0,0\rangle$, $|1,1\rangle$, $|1,-1\rangle$, and $|1,0\rangle$, where the first number represents the orbital momentum quantum number and the second one is the projection along the z direction. Details of the Hamiltonian construction can be found in the Supplemental Material.

To include the SOI, we use the standard form describing the spin-orbit coupling arising from the interaction with the nucleus $H_{\rm SOI} = T_X(\frac{L_+ \otimes s_- + L_- \otimes s_+}{2} + L_z \otimes s_z)$, where X is either Pb or S. The last term modifies the diagonal elements of the self-energy for $|1, \pm 1\rangle$ by adding (subtracting) $T_X/2$ if L_z and s_z point in the same (opposite) direction. The first term couples $|1,1\rangle \otimes |\downarrow\rangle$ with $|1,0\rangle \otimes |\uparrow\rangle$ and $|1,-1\rangle \otimes |\uparrow\rangle$ with $|1,0\rangle \otimes |\downarrow\rangle$ with the coupling strength $T_X/\sqrt{2}$.

The first high-symmetry point that we examine is the M point, located at $(\pi/2, \pi/2)$ in the Brillouin zone. At the M point the full Hamiltonian H can be decomposed into several blocks, and the Hamiltonian describing the two lowest conduction bands (C1, C2) and the third valence band (V3) is given by

$$H_b = \begin{pmatrix} \varepsilon_p^{\rm S} + \frac{T_{\rm S}}{2} & \mp 4i\alpha^2\Delta & 0 \\ \pm 4i\alpha^2\Delta & \varepsilon_p^{\rm Pb} - \frac{T_{\rm Pb}}{2} & \frac{T_{\rm Pb}}{\sqrt{2}} \\ 0 & \frac{T_{\rm Pb}}{\sqrt{2}} & \varepsilon_p^{\rm Pb} \end{pmatrix}. \tag{1}$$

At the M point, the degenerate wave functions (labeled as 1 and 2) describing the lowest conduction band C1 are given by

$$\begin{aligned} |\Psi_1\rangle = {}& iA|1,1\rangle \otimes |\uparrow\rangle_{\rm S} + B|1,-1\rangle \\ & \otimes |\uparrow\rangle_{\rm Pb} + C|1,0\rangle \otimes |\downarrow\rangle_{\rm Pb}, \\ |\Psi_2\rangle = {}& -iA|1,-1\rangle \otimes |\downarrow\rangle_{\rm S} + B|1,1\rangle \\ & \otimes |\downarrow\rangle_{\rm Pb} + C|1,0\rangle \otimes |\uparrow\rangle_{\rm Pb}, \end{aligned} \tag{2}$$

where A, B, and C are real numbers. The other block H_a describing the highest valence (V1) band has a very similar form to Eq. (1), but where Pb and S are interchanged.

The degeneracy breaking term γ is given by

$$\gamma = \langle \Psi_1 | H | \Psi_2 \rangle = 2i \sin(2\theta)\Delta k e^{i\phi} AC, \tag{3}$$

where θ is the structure buckling angle, where $\Delta = V_{pp\sigma} - V_{pp\pi}$ (V is the hopping parameter between the S and Pb atom; see Supplemental Material), and $ke^{i\phi} = k_x + ik_y$. This leads to a linear dispersion for small k, as expected. Defining $\lambda \equiv 2\sin(2\theta)\Delta AC$, we can write the effective Hamiltonian
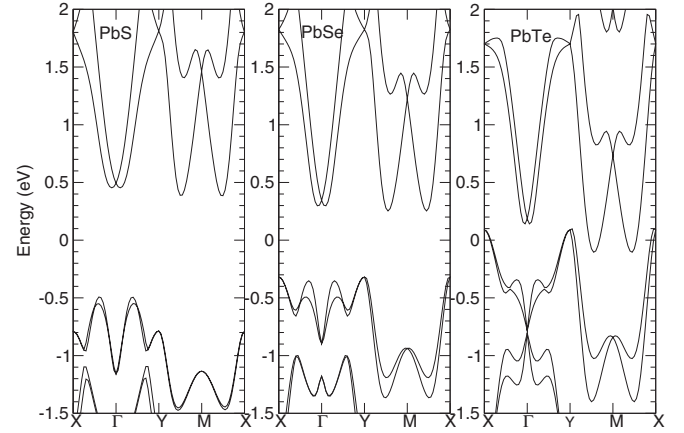

FIG. 2. Band structures of buckled PbS, PbSe, and PbTe with spin-orbit interaction included. Fermi energy is set to be zero. All buckled lead chalcogenides have large Rashba splitting in the conduction band. In the highest valence bands, however, the Rashba splitting is smaller for compounds containing lighter chalcogen species.

describing the lowest conduction band as

$$H_{\rm eff} = \lambda[\vec{k} \times \vec{\sigma}] \cdot \hat{z}, \tag{4}$$

where $\vec{\sigma} = (\sigma_x, \sigma_y, \sigma_z)$, which is the Rashba Hamiltonian. The eigenstates are $|\psi_{\rm I,II}\rangle = |\Psi_1\rangle \pm ie^{-i\phi}\frac{|\lambda|}{\lambda}|\Psi_2\rangle$.

It is clear from Eq. (1) that the SOI mixes the p_z orbital with other in-plane orbitals of atoms with the same species; however, SOI by itself does not lift the degeneracy because SOI is independent of k. For instance, the band structure of *planar* PbS obtained by DFT, including the SOI, does not show spin splitting [Fig. 1(b)]. The inversion symmetry breaking term originated from the buckling couples the p_z of Pb and the in-plane p orbitals of S atoms; this term results in the spin splitting with Rashba-like dispersion [see Eq. (3)]. Taking $T_{\rm Pb} \gg T_{\rm S}$ and solving the Hamiltonian H_b perturbatively, one can show that, to the first leading order, $AC \sim T_{\rm Pb}$. These two consequences are consistent with our DFT results: spin splitting occurs when both SOI and θ are not zero.

While the same arguments hold for H_a, which describes the valence band, we do not observe a substantial SOI-induced splitting in PbS [see Fig. 1(c)]. This is because the sulfur atom has a much smaller atomic SOI than the Pb atom, leading to a weaker mixing of orbitals, suppressing the AC term in the equation above. As shown in Fig. 2, PbTe and PbSe, however, have large spin splitting in both the conduction and valence bands because Te and Se are relatively much heavier than S (stronger SOI) [32].

Similarly to the M point, one can perform a low-k expansion around the Γ point for the Hamiltonian matrix (see Supplemental Material). Because there are more nonvanishing coupling terms at the center of the Brillouin zone, the Hamiltonian does not reduce as well to smaller independent blocks as it does at the M point. Nevertheless, it is possible to show that in buckled structures, there is a linear term breaking the degeneracy of the conduction band.
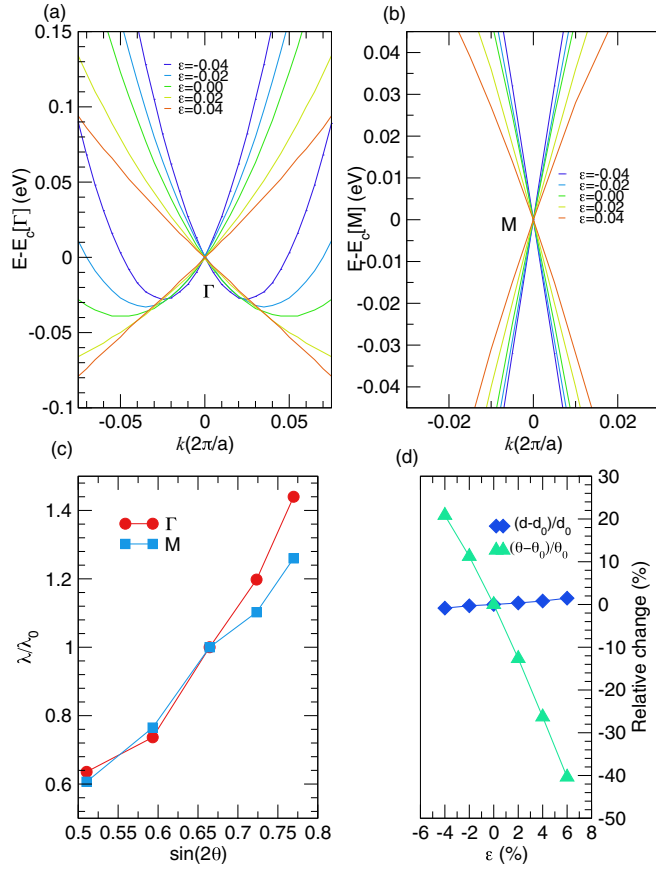
FIG. 3. Evolution of band structure around Γ (a) and M (b) with application of biaxial strains. Energy is subtracted by energy at Γ (M) for comparative purposes. (c) λ scaled by its unstrained value λ_0 as a function of $\sin 2\theta$. λ increases with increasing buckling angle, which is consistent with tight-binding analysis. (d) Relative changes in buckling angle θ and bond distance d as a function of biaxial strain ϵ.

We have found the relevant parameters to tune the band splitting from the tight-binding (TB) formulation. Clearly the hopping parameters depend on both the bond distance and the buckling angle. Since these two quantities are often strain dependent, it is natural to ask whether it is possible to tune the hopping parameters using strain. Our DFT simulations showed that under biaxial strains the bond distance changes by only 1% while the buckling angle changes by roughly 30% at a biaxial strain of 6% (shown in Fig. 3).

We obtain λ by taking the derivative of energy dispersion $\lambda = \frac{\partial E}{\partial k}$ at Γ and M. As shown in Fig. 3(c), λ increases with increasing θ, consistent with our TB formulation [see Eq. (3)]. Note that λ is not linear with $\sin 2\theta$ because A and C also depend on θ. Our DFT results show that, relative to its unstrained value λ_0, λ can increase by more than 20% when compressed by 4% or decrease by 20% when stretched by 4%. The apparent variations of λ show that PbS is a tunable spin-splitting material.

Spin and orbital texture. Lastly, we investigate the orbital texture of PbS as it has been shown that TIs and hexagonal 3D Rashba materials have orbital switching at the Dirac point [13–16]. Here we can do an analysis for monolayers with

square symmetry by transforming our basis to radial p_r and tangential p_t orbitals: $|1,1\rangle = -e^{i\phi}|p_r\rangle + i|p_t\rangle$, $|1,-1\rangle = e^{-i\phi}|p_r\rangle - i|p_t\rangle$, and $|1,0\rangle = |p_z\rangle$. In this basis the upper and bottom wave functions can be written as

$$
\begin{aligned}
|\psi_{\mathrm{I,II}}\rangle = {} & C|p_z\rangle \otimes |\pm\rangle_{\mathrm{Pb}} \mp i\frac{B}{\sqrt{2}}|p_r\rangle \otimes |\pm\rangle_{\mathrm{Pb}} \\
& \pm \frac{B}{\sqrt{2}}|p_t\rangle \otimes |\mp\rangle_{\mathrm{Pb}} \mp i\frac{A}{\sqrt{2}}e^{-2i\phi}|p_r\rangle \otimes |\mp_3\rangle_{\mathrm{S}} \\
& \pm \frac{A}{\sqrt{2}}e^{-2i\phi}|p_t\rangle \otimes |\pm_3\rangle_{\mathrm{S}},
\end{aligned} \tag{5}
$$

where $|+_n\rangle = \frac{1}{\sqrt{2}}\binom{\frac{|\lambda|}{\lambda}ie^{-in\phi}}{1}$ is clockwise in-plane spin and $|-_n\rangle = \frac{1}{\sqrt{2}}\binom{-\frac{|\lambda|}{\lambda}ie^{-in\phi}}{1}$ is counterclockwise in-plane spin.

In the upper band of PbS the radial component of the Pb atom couples to the clockwise spin while the tangential component couples to the counterclockwise spin, as shown schematically in Fig. 4. As it passes through the band crossing point (Dirac point) right at the M point, where the upper band and lower band meet, the tangential component now couples to the counterclockwise spin. This switching is similar to what has been observed in TIs [13,14] and hexagonal bulk Rashba materials [15,16]. The difference is that the radial and tangential components contribute equally and cancel out, and thus the net in-plane spin texture comes from the p_z orbital only. This suggests that the orbital texture is not always polarized and thus the orbital polarization depends on the crystal symmetry of the material.

From the TB results, we found that the direction of the spin is given by $\langle\psi_{\mathrm{I,II}}|\hat{\sigma}|\psi_{\mathrm{I,II}}\rangle = \pm\frac{|\lambda|}{\lambda}(\sin\phi, -\cos\phi, 0)$. We can see that the spin texture is helical and depends on the direction of the buckling (inversion symmetry breaking term λ). Notice that the PbS-b has a degenerate structure as the polarization vector in the z direction defined as $d_z = z(\mathrm{Pb}) - z(\mathrm{S})$ can be positive or negative (sign of λ), as shown in Fig. 4(c). Thus, the in-plane spin texture can be reversed when λ is negative (PbS buckled in the opposite direction). This is confirmed by our DFT results shown in Fig. 4(c). While the coefficients A, B, and C in Eq. (2) are material dependent, the orbital texture is independent of the direction of the buckling. These findings are in agreement with the very recent work on hexagonal 3D Rashba BiTeI [15].

Conclusion. In summary, using first-principles calculations based on density functional theory, we have found a class of 2D materials (lead chalcogenides) possessing a tunable giant Rashba splitting with a characteristic orbital and spin texture in an energy range close to the band-gap edge. Based on our tight-binding analysis, we found that the atomic composition and buckling angle are the two key parameters controlling the Rashba effects. First, the atomic composition plays an important role as the SOI is the parameter that mixes the in-plane and out-of-plane orbitals. With the recent success in creating Janus (polar) transition-metal dichalcogenide mono-layers [33] and few-layer SnTe and PbTe [18] via atomic layer deposition techniques, the growth of buckled polar materials
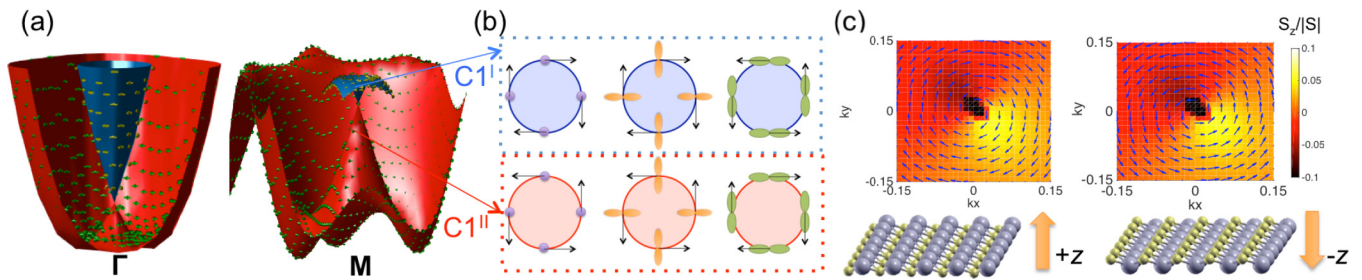
FIG. 4. (a) Band plots of the first (C1^{II}) and second (C1^{I}) lowest conduction band near the Γ and M points. Clockwise (counterclockwise) spin textures are represented by the yellow (green) arrows. Near the band crossing (inner Dirac cone), the upper and lower bands have opposing helical spin texture similar to the Rashba spin texture. (b) Corresponding schematic orbital spin texture of the Pb atom at the M point. The radial p_r and tangential p_t have opposite spin orientation, and they cancel each other. Spin helicity is flipped after passing through the Dirac point while the orbital compositions are still the same. (c) Two-dimensional plot of spin polarizations near M. The color plot shows the projection of spin along the z direction. Clearly, the out-of-plane spin components are small. The direction of spin polarizations is reversed when the buckling direction is reversed.

like PbS, PbSe, and PbTe should also be achievable using existing technology.

In buckled PbS monolayers, the Rashba coefficient depends on the degree of buckling, and the orientation of the helical in-plane spin depends on the direction of the buckling. As we have shown in DFT simulations, this buckling can be controlled through the application of moderate strains of $\leqslant 10\%$, which are achievable in the current 2D experiments [34,35]. A similar system showing such tunability is LaOBiS$_2$ [36]. In addition to mechanical strains, the electric polarization (direction of buckling) can be switched as PbS is ferroelectric. And thus PbS spin texture can be switched in a nonvolatile way which is similar to recently found ferroelectric Rashba semiconductors GeTe [37]. Further, we also found orbital-spin texture switching in buckled PbS. Our results suggest that the orbital-spin switching at the Dirac point is not exclusive to TIs and the orbital texture is not always polarized, as it depends on the crystal symmetry of the material. Our unifying framework based on tight binding provides design principles and orbital-spin texture manipulations which will be important for the development of new devices.

[1] K. Ishizaka, M. S. Bahramy, H. Murakawa, M. Sakano, T. Shimojima, T. Sonobe, K. Koizumi, S. Shin, H. Miyahara, A. Kimura, K. Miyamoto, T. Okuda, H. Namatame, M. Taniguchi, R. Arita, N. Nagaosa, K. Kobayashi, Y. Murakami, R. Kumai, Y. Kaneko, Y. Onose, and Y. Tokura, Nat. Mater. **10**, 521 (2011).

[2] M. Sakano, M. S. Bahramy, A. Katayama, T. Shimojima, H. Murakawa, Y. Kaneko, W. Malaeb, S. Shin, K. Ono, H. Kumigashira, R. Arita, N. Nagaosa, H. Y. Hwang, Y. Tokura, and K. Ishizaka, Phys. Rev. Lett. **110**, 107204 (2013).

[3] Y. Kim, C. L. Kane, E. J. Mele, and A. M. Rappe, Phys. Rev. Lett. **115**, 086802 (2015).

[4] J. Liu, X. Qian, and L. Fu, Nano Lett. **15**, 2657 (2015).

[5] X. Zhang, Q. Liu, J.-W. Luo, A. J. Freeman, and A. Zunger, Nat. Phys. **10**, 387 (2014).

[6] H. Min, J. E. Hill, N. A. Sinitsyn, B. R. Sahu, L. Kleinman, and A. H. MacDonald, Phys. Rev. B **74**, 165310 (2006).

[7] H. Yuan, M. S. Bahramy, K. Morimoto, S. Wu, K. Nomura, B.-J. Yang, H. Shimotani, R. Suzuki, M. Toh, C. Kloc, X. Xu, R. Arita, N. Nagaosa, and Y. Iwasa, Nat. Phys. **9**, 563 (2013).

[8] A. Avsar, J. Y. Tan, T. Taychatanapat, J. Balakrishnan, G. K. W. Koon, Y. Yeo, J. Lahiri, A. Carvalho, A. S. Rodin,

E. C. T. O'Farrell, G. Eda, A. H. Castro Neto, and B. Özyilmaz, Nat. Commun. **5**, 4875 (2014).

[9] D. D. Sante, A. Stroppa, P. Barone, M.-H. Whangbo, and S. Picozzi, Phys. Rev. B **91**, 161401 (2015).

[10] Q.-F. Yao, J. Cai, W.-Y. Tong, S.-J. Gong, J.-Q. Wang, X. Wan, C.-G. Duan, and J. H. Chu, Phys. Rev. B **95**, 165401 (2017).

[11] Y. Zhang, K. He, C.-Z. Chang, C.-L. Song, L.-L. Wang, X. Chen, J.-F. Jia, Z. Fang, X. Dai, W.-Y. Shan, S.-Q. Shen, Q. Niu, X.-L. Qi, S.-C. Zhang, X.-C. Ma, and Q.-K. Xue, Nat. Phys. **6**, 584 (2010).

[12] A. S. Rodin, P. Z. Hanakata, A. Carvalho, H. S. Park, D. K. Campbell, and A. H. C. Neto, arXiv:1703.04713.

[13] Y. Cao, J. A. Waugh, X.-W. Zhang, J.-W. Luo, Q. Wang, T. J. Reber, S. K. Mo, Z. Xu, A. Yang, J. Schneeloch, G. D. Gu, M. Brahlek, N. Bansal, S. Oh, A. Zunger, and D. S. Dessau, Nat. Phys. **9**, 499 (2013).

[14] H. Zhang, C.-X. Liu, and S.-C. Zhang, Phys. Rev. Lett. **111**, 066801 (2013).

[15] Q. Liu, X. Zhang, J. A. Waugh, D. S. Dessau, and A. Zunger, Phys. Rev. B **94**, 125207 (2016).

[16] L. Bawden, J. M. Riley, C. H. Kim, R. Sankar, E. J. Monkman, D. E. Shai, H. I. Wei, E. B. Lochocki, J. W. Wells, W. Meevasana, T. K. Kim, M. Hoesch, Y. Ohtsubo, P. Le Fèvre, C. J. Fennie, K. M. Shen, F. Chou, and P. D. C. King, Sci. Adv. **1**, e1500495 (2015).

[17] W. Wan, Y. Yao, L. Sun, C.-C. Liu, and F. Zhang, Adv. Mater. **29**, 1604788 (2017).

[18] K. Chang, J. Liu, H. Lin, N. Wang, K. Zhao, A. Zhang, F. Jin, Y. Zhong, X. Hu, W. Duan, Q. Zhang, L. Fu, Q.-K. Xue, X. Chen, and S.-H. Ji, Science **353**, 274 (2016).

[19] Chang *et al.* reported PbTe data in the Supplementary Material.

[20] P. Giannozzi, S. Baroni, N. Bonini, M. Calandra, R. Car, C. Cavazzoni, D. Ceresoli, G. L. Chiarotti, M. Cococcioni, I. Dabo, A. D. Corso, S. de Gironcoli, S. Fabris, G. Fratesi, R. Gebauer, U. Gerstmann, C. Gougoussis, A. Kokalj, M. Lazzeri, L. Martin-Samos, N. Marzari, F. Mauri, R. Mazzarello, S. Paolini, A. Pasquarello, L. Paulatto, C. Sbraccia, S. Scandolo, G. Sclauzero, A. P. Seitsonen, A. Smogunov, P. Umari, and R. M. Wentzcovitch, J. Phys.: Condens. Matter **21**, 395502 (2009).

[21] J. P. Perdew, K. Burke, and M. Ernzerhof, Phys. Rev. Lett. **77**, 3865 (1996).

[22] H. J. Monkhorst and J. D. Pack, Phys. Rev. B **13**, 5188 (1976).

[23] R. D. King-Smith and D. Vanderbilt, Phys. Rev. B **47**, 1651 (1993).

[24] P. Z. Hanakata, A. Carvalho, D. K. Campbell, and H. S. Park, Phys. Rev. B **94**, 035304 (2016).

[25] R. Fei, W. Kang, and L. Yang, Phys. Rev. Lett. **117**, 097601 (2016).

[26] H. Wang and X. Qian, 2D Mater. **4**, 015042 (2017).

[27] See Supplemental Material at http://link.aps.org/supplemental/10.1103/PhysRevB.96.161401 for details on the potential energy surface, projected density of states, full Hamiltonian, and optimized geometrical parameters of PbSe and PbTe.

[28] S. P. Beckman, X. Wang, K. M. Rabe, and D. Vanderbilt, Phys. Rev. B **79**, 144124 (2009).

[29] B. Radisavljevic, A. Radenovic, J. Brivio, V. Giacometti, and A. Kis, Nat. Nanotechnol. **6**, 147 (2011).

[30] M. Liebmann, C. Rinaldi, D. D. Sante, J. Kellner, C. Pauly, R. N. Wang, J. E. Boschker, A. Giussani, S. Bertoli, M. Cantoni, L. Baldrati, M. Asa, I. Vobornik, G. Panaccione, D. Marchenko, J. Sánchez-Barriga, O. Rader, R. Calarco, S. Picozzi, R. Bertacco, and M. Morgenstern, Adv. Mater. **28**, 560 (2016).

[31] Data can be found in the Supplemental Material.

[32] The optimized geometrical parameters of buckled PbTe and PbSe monolayers are tabulated in the Supplemental Material.

[33] A.-Y. Lu, H. Zhu, J. Xiao, C.-P. Chuu, Y. Han, M.-H. Chiu, C.-C. Cheng, C.-W. Yang, K.-H. Wei, Y. Yang, Y. Wang, D. Sokaras, D. Nordlund, P. Yang, D. A. Muller, M.-Y. Chou, X. Zhang, and L.-J. Li, Nat. Nanotechnol. **12**, 744 (2017).

[34] D. Lloyd, X. Liu, J. W. Christopher, L. Cantley, A. Wadehra, B. L. Kim, B. B. Goldberg, A. K. Swan, and J. S. Bunch, Nano Lett. **16**, 5836 (2016).

[35] H. H. Pérez Garza, E. W. Kievit, G. F. Schneider, and U. Staufer, Nano Lett. **14**, 4107 (2014).

[36] Q. Liu, Y. Guo, and A. J. Freeman, Nano Lett. **13**, 5264 (2013).

[37] D. D. Sante, P. Barone, R. Bertacco, and S. Picozzi, Adv. Mater. **25**, 509 (2013).